



Contents lists available at ScienceDirect



Numerical and experimental study of radial segregation of bi-disperse particles in a quasi-two-dimensional horizontal rotating drum

Zhichao Hou, Yongzhi Zhao*

Institute of Process Equipment, College of Energy Engineering, Zhejiang University, Hangzhou 310027, China

ARTICLE INFO

Article history:

Received 6 December 2018

Received in revised form 11 February 2019

Accepted 23 September 2019

Available online xxx

Keywords:

Discrete element method

Radial segregation

Granular flow

Rotating drum

Reverse segregation

ABSTRACT

Radial segregation easily occurs in a horizontal rotating drum partially filled with particles of different properties under various operational conditions. DEM (discrete element method) simulations and experiments were combined together to investigate the segregation of bi-disperse particles of the same density but unequal sizes in a quasi-two-dimensional horizontal rotating drum. A linear spring-dashpot model was adopted in simulations. An easy and effective image analysis was conducted for the segregation/mixing of particles of different sizes. By comparing the repose angles, degrees of segregation, and particular phenomenon ("sun pattern" and reverse segregation) in simulations under different operating conditions with those in experiments, the discrete-element model is verified. The effects of rotational speed and volume ratio on radial segregation are also considered systematically. From an analysis of the results of experiments and simulations, the degree of segregation generally decreases with increasing rotational speed, whereas the volume ratio shows different influences on segregation in different flow regimes. Moreover, the mechanism underlying the reverse segregation in the cataracting regime has been clarified as well.

© 2019 Chinese Society of Particuology and Institute of Process Engineering, Chinese Academy of Sciences. Published by Elsevier B.V. All rights reserved.

Introduction

In process industries, homogeneity in products of two or more components is often desired and proper mixing is important. However, segregation easily occurs when particles differ in size, density or other properties. Typical solutions to combat segregation mainly fall into two classes: changing the particles, which may involve balancing differences in size and density; changing the process, which may involve geometrical changes or operational changes (Ottino & Lueptow, 2008). The horizontal rotating drum is widely used as a mixing device in chemical, pharmaceutical, ceramic, metallurgical and food industries (Herz, Sonavane, Specht, Bensmann, & Walzel, 2009; Jain, Ottino, & Lueptow, 2002; Nafsun et al., 2017). Investigating segregation in this device is essential both in practice and in theory.

The experimental approach is fundamental in investigating segregation in the drum. In experiments involving mixing binary granular media in a rotating drum, sun patterns were found (Gray & Hutter, 1997; Hill, Gioia, & Amaravadi, 2004; Hill, Gioia, Amaravadi, & Winter, 2005; Pereira, Pucilowski, Liffman, & Cleary, 2011; Zuriguel, Gray, Peixinho, & Mullin, 2006; Zuriguel, Peixinho,

& Mullin, 2009). From experiments and a continuum model, Fiedor and Ottino (2005) presented an analysis on size segregation in dry and wet granular systems in time-periodically forced quasi-two-dimensional tumblers. Jain, Ottino, and Lueptow (2005) conducted experiments concerning the combined effects of size and density on segregation and mixing in circular and noncircular tumblers. In addition, Santomaso, Olivi, and Canu (2005) reported that the mixing kinetics of granular materials in drums operated in the cataracting regime satisfy a diffusion model. Nityanand, Manley, and Henein (1986) presented some experimental observations of radial segregation arising from size differences involving reverse segregation, which appears at high rotational speeds (To clarify, small particles normally segregate from big particles and move into the core of the drum, where they were previously mixed, and flow with the rotating drum; however, when small particles are segregated at the periphery of the drum, this process is referred to as reverse segregation.). In that study, reverse segregation was interpreted to mean that small particles are easily centrifuged to the wall of the cylinder. With a similar interpretation, Turner and Nakagawa (2000) explained the same phenomenon appearing in a nearly filled horizontal cylinder. Thomas (2000) reported reverse segregation that depends on size ratio and volume fraction and attributed it to the interaction between geometry and gravitation. Without experiments, these particular phenomena and segregation/mixing mechanisms would not have been found and elucidated; they

* Corresponding author.

E-mail address: yzzhao@zju.edu.cn (Y. Zhao).

had provided insights in regard to the basic theories of particle systems. Furthermore, analytical models from mathematics and physics were also employed in understanding particle mixing and segregation (Gray, 2010; Khakhar, McCarthy, Shinbrot, & Ottino, 1997; McCarthy, Shinbrot, Metcalfe, Wolf, & Ottino, 1996; Metcalfe, Shinbrot, McCarthy, & Ottino, 1995; Prigozhin & Kalman, 1998).

Other than experimental and theoretical methods, numerical simulation is an effective way to gain insights from granular systems, benefitting from the enormous leap forward in computational speeds. The arrival of the discrete element method (DEM) made it possible to simulate particle systems and represents a significant advance for the field of particle systems (Bridgwater, 2012). Cundall and Strack (1979) pioneered the work on DEM. Since then, DEM simulations have played a key role in the study of granular flow, mixing, and segregation. Dury and Ristow (1997) described the size segregation of a binary mixture of granular material in a half filled two-dimensional rotating drum using DEM. In addition, through DEM, Alchikh-Sulaiman, Alian, Ein-Mozaffari, Lohi, and Upreti (2016) studied the mixing of mono-disperse, bi-disperse, tri-disperse, and poly-disperse solid particles in a rotary drum. DEM is useful in constructing the continuum theory of particles as well. For example, instead of arbitrarily fitting various adjustable parameters, Fan, Schlick, Umbanhowar, Ottino, and Lueptow (2014) collected information on kinematic parameters from DEM simulations to develop their continuum-based theoretical model. In addition, Arntz et al. (2008, 2014) numerically investigated the impact of particles' properties such as radius, density, and mass, and drum operating parameters such as rotational speed and fill level on granular mixing and segregation in a horizontal rotating drum. However, the number of particles in their simulation was not enough to elucidate the cause of reverse segregation occurred in the cataracting regime. To validate their DEM code, Komossa, Wirtz, Scherer, Herz, and Specht (2014) presented a comparison of experiments and DEM simulations with different Froude numbers, dynamic angles of repose, thicknesses of the active layer, and particle velocities on the bed. Nevertheless, the validation was demonstrated only for the rolling regime. To the best of our knowledge, little has been done on the influences of rotational speed and of volume ratio of small to big particles on bi-disperse segregation in a rotary drum.

As described above, radial segregation has been intensively investigated by either experiments or simulations. Considering that information of particles in the bulk is hard to obtain through experimental approaches and simulations are also needed to be validated, a combination of these two means is necessary and hence implemented in our study. Furthermore, in the simulations of bi-disperse particles in a horizontal rotating drum, nearly 200,000 particles were employed, which is sufficient to gain more reliable insights and to investigate the full range of drum speeds, both numerically and experimentally, without the restriction to a single flow regime. Moreover, an effective image analysis was applied that can recognize and locate particles of different sizes on a large scale to measure the degree of segregation of particles in the drum. With this advantage, the DEM model adopted in numerical simulation was validated. Moreover, the influences of rotational speed over a broad range and the volume ratio of small-to-big particles on bi-disperse radial segregation in a rotary drum have been investigated systematically, and the mechanism of reverse segregation occurring in the cataracting regime is clarified as well.

Discrete element model and simulation conditions

In our DEM simulations, the particles are subjected to the force of gravity and contact forces arising from collisions, which were decomposed into a normal contact force \mathbf{F}_n and a tangential

contact force \mathbf{F}_t . Various contact force models have been proposed, and linear models are mainly applied in DEMs. The most commonly used linear model is called the linear spring-dashpot model (Cundall & Strack, 1979). More complicated models are the Hertz–Mindlin–Deresiewicz model (Hertz, 1896; Mindlin & Deresiewicz, 1953; Mindlin, 1949) and the non-linear models (Thornton, Cummins, & Cleary, 2013; Walton & Braun, 1986; Walton, 1993). For simplicity and robustness, we adopted a linear spring-dashpot model. The motion of particles follows Newton's second law of motion. For particle i of mass m_i and moment of inertia I_i under the action of another particle j , its translational motion satisfies

$$m_i \frac{d\mathbf{v}_i}{dt} = m_i \mathbf{g} + \sum_{j=1}^{n_i} (\mathbf{F}_{n,ij} + \mathbf{F}_{t,ij}), \quad (1)$$

where \mathbf{v} denotes the translational velocity, \mathbf{g} the gravitational acceleration. And the rotational motion of particle i obeys

$$I_i \frac{d\boldsymbol{\omega}_i}{dt} = \sum_{j=1}^{n_i} \mathbf{T}_{t,ij}, \quad (2)$$

where $\boldsymbol{\omega}$ is the rotational velocity, and \mathbf{T}_t is the moment originating from the tangential contact force; in both equations n_i is the number of particles in contact with particle i .

This model covers the normal contact force, the tangential contact force, and torque, each of which may be simplified as a combination of a spring, a damper, and a slider. These forces and moments can be stated as

$$\mathbf{F}_{n,ij} = -k_n \delta_n - \eta_n \mathbf{v}_{n,ij} \quad (3)$$

$$\mathbf{F}_{t,ij} = -k_t \delta_t - \eta_t \mathbf{v}_{t,ij} \quad (4)$$

where \mathbf{v}_n and \mathbf{v}_t are the normal and tangential relative velocities, respectively, δ_n and δ_t are the normal and tangential deformation displacements, and subscripts n and t signify respectively the normal and tangential directions. Once the force condition

$$|\mathbf{F}_{t,ij}| > f_s |\mathbf{F}_{n,ij}| \quad (5)$$

is met, the tangential contact force is given by the Coulomb friction model,

$$\mathbf{F}_{t,ij} = -f_s |\mathbf{F}_{n,ij}| \delta_t / |\delta_t|. \quad (6)$$

In this work, only the tangential contact torque is taken into account,

$$\mathbf{T}_{t,ij} = \mathbf{L}_i \times \mathbf{F}_{t,ij}, \quad (7)$$

where \mathbf{L} is the distance from the center of the sphere to the contact point.

As suggested in Ting and Corkum (1992), the coefficient of damping η can be obtained from the coefficient of restitution e and other parameters (see Table 1). In simulations, to ensure the stability and accuracy of the algorithm, the time step should not be too long. There exists a critical time step that must not be exceeded in the corresponding computation. In general, the critical time step is set as one tenth of the elastic collision period, which is the minimum of the normal and tangential collision periods (Ting & Corkum, 1992).

Employing the above mathematical model, a self-developed DEM code named DEMSLab, which is capable of simulating the behaviors of bulk materials of various geometries, is used in investigating the radial segregation of bi-disperse particles in a horizontal rotating drum. The parameter settings used in simulations are listed in Table 2.

Table 1

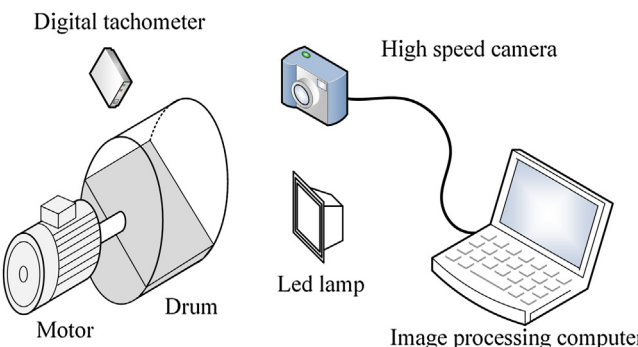
Collision damping coefficients of particle-particle and particle-wall.

Damping coefficient	Equation	Particle-particle	Particle-wall
e ≠ 0	e = 0		
Normal damping	$\eta_n = 2 \sqrt{mk_n} \frac{\ln(1/e_n)}{\sqrt{\pi^2 + \ln^2(1/e_n)}}$	$\eta_n = 2 \sqrt{mk_n}$	$m = \frac{m_i m_j}{m_i + m_j}$
Tangential damping	$\eta_t = 2 \sqrt{mk_t} \frac{\ln(1/e_t)}{\sqrt{\pi^2 + \ln^2(1/e_t)}}$	$\eta_t = 2 \sqrt{mk_t}$	$m = \frac{2}{7} \frac{m_i m_j}{m_i + m_j}$

Table 2

Simulation parameters.

Parameter	Value
Drum, D × L (mm)	200 × 10
Diameter of big particles (mm)	1.6–2.0
Diameter of small particles (mm)	0.8–0.9
Particle density (kg/m ³)	2,500
Total number of particles	100,000–200,000
Coefficient of restitution	0.9
Coefficient of sliding friction between particle and particle	0.4
Coefficient of sliding friction between particle and wall	0.9
Coefficient of sliding friction between particle and faceplate	0.4
Filling fraction	0.5
Rotational speed (rpm)	2, 4, 8, 16, 32, 56, 80
Volume ratio of small particles to big particles	1, 1/2, 1/3
Time step (s)	2 × 10 ⁻⁵

**Fig. 1.** Schematic of the experimental setup.

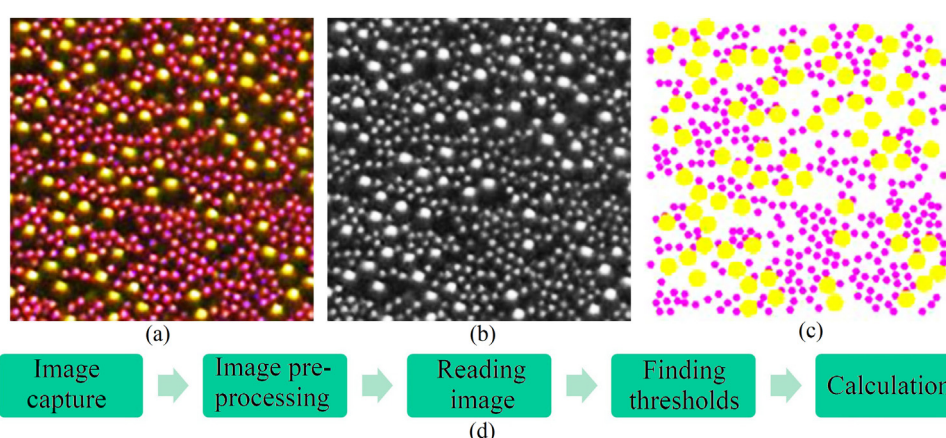
Experimental method

The experimental setup (Fig. 1) includes a home-made rotary drum of diameter 200 mm covered with a transparent acrylic plate

on the front end and a steel plate on the back end. An acrylic plate was chosen for its good transparency to observe the mixing of particles directly. Large golden glass spheres (1.6–2 mm) and small mauve glass spheres (0.8–0.9 mm) were mixed uniformly at volume ratios (small to large) of 1, 1/2, and 1/3 to fill in 50% of the drum's chamber. The drum was rotated using a stepper motor at rotational speeds of 2, 4, 8, 16, 32, 56, 80 rpm so that the particle motion in the drum covers all flow regimes. The free surface of the particle bed is horizontally placed before the drum is rotated. Illuminated by a LED lamp, radial segregation is captured in video using an industrial high-speed camera with a shutter speed of 0.005 ms, a maximum frame rate of 163 frames per second, and a resolution of 1920 × 1200 pixels.

In the experiment, some details need noting. One is the thickness of the drum is 10 mm, which is about 5 times the size of the largest particle, and the drum diameter (200 mm) is an order of magnitude larger than the thickness of the drum. This is to ensure the drum is quasi-two-dimensional where the axial segregation of the particles can be restricted as far as possible and thereby confine the focus to radial segregation. In addition, the surface of the drum's cylindrical wall was roughened sufficiently to prevent the particle bed from sliding before it reached its max repose angle. Finally, as electrostatic forces are not considered in this study, static electricity generated mainly between moving glass particles and the drum ends is suppressed. For this reason, a transparent anti-static film was added between the wall and the front plate, and the back plate was made of steel.

Compared with traditional sampling methods (Prigozhin & Kalman, 1998) that obtain the degree of mixing or segregation of the granular materials, image analysis methods are noninvasive. Based on image processing techniques, the variation in color concentration is often used to evaluate the mixing state, which is not robust especially when the particles fade easily. In this study, we calculated the particle concentration by identifying large and small particles directly based on the brightness of areas of different sizes for big and small particles when they are illuminated with relatively strong and uniform light (Fig. 2(a) and (b)). The different-sized areas

**Fig. 2.** Image analysis method: (a) subimage sample in RGB, (b) subimage sample in grayscale, (c) distinguishing particles in the sample, and (d) procedures in image analysis.

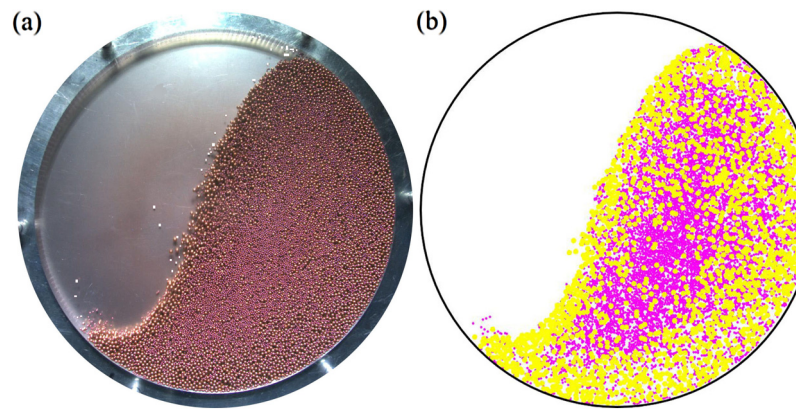


Fig. 3. Snapshot of the full field of view of particles obtained from: (a) experiment and (b) corresponding identification results of the experiment.

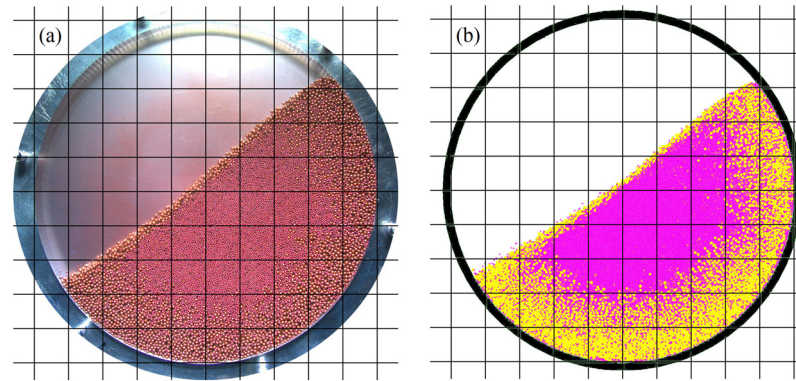


Fig. 4. Grid partition for the calculations of Lacey mixing index obtained from (a) experiment and (b) simulation.

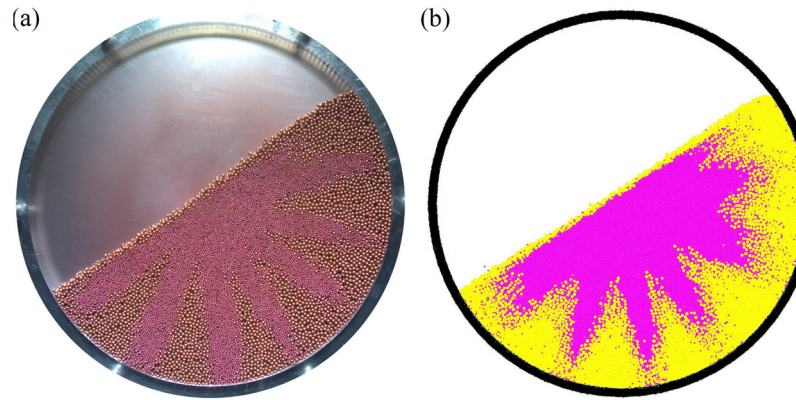


Fig. 5. “Sun pattern” snapshots with volume ratio of 1 and rotational speed of 2 rpm obtained from: (a) experiment and (b) simulation.

of relative brightness help to locate and distinguish particles of different sizes and subsequently to obtain the variation in particle concentrations. The developed image analysis method of our experiment (Fig. 2(d)) mainly consists of five steps:

Step 1: Image capture—The LED lamp was placed at an incline above the drum to provide ample light needed for taking pictures. The high-speed camera is directly in front of the drum, with the center lines of the lens and the drum coinciding. The distance between the camera lens and the drum needs to be adjusted to an appropriate length so that the whole drum nearly occupies the whole viewing frame. The camera's settings—brightness, exposure, sharpness, saturation, shutter, and frame rate—were adjusted according to the granular flow regime to acquire sharp images. After these adjustments, the drum and camera were positioned to ensure the images obtained were all of the same size.

Step 2: Image pre-processing—The main purpose is to remove imaging noise for the next step. The noise from the previous step includes mainly the periphery of the drum and the background not obscured by particles. The periphery of the drum is de-framed and the unoccupied background is eliminated using an image processing tool.

Step 3: Reading image—The classification of pixels is completed using the Image Processing Toolbox (MATLAB).

Step 4: Finding thresholds—Here, the thresholds are defined by how many brighter pixels are involved in the brighter areas for large and small particles, respectively, and the range of average gray values that distinguish the brighter areas from the whole particle surface. In our experiment, for the 1920×1200 -pixel image captured, each large particle (1.6–2 mm) covers a brighter area of approximately 16 pixels, and each small particle (0.8–0.9 mm) cov-

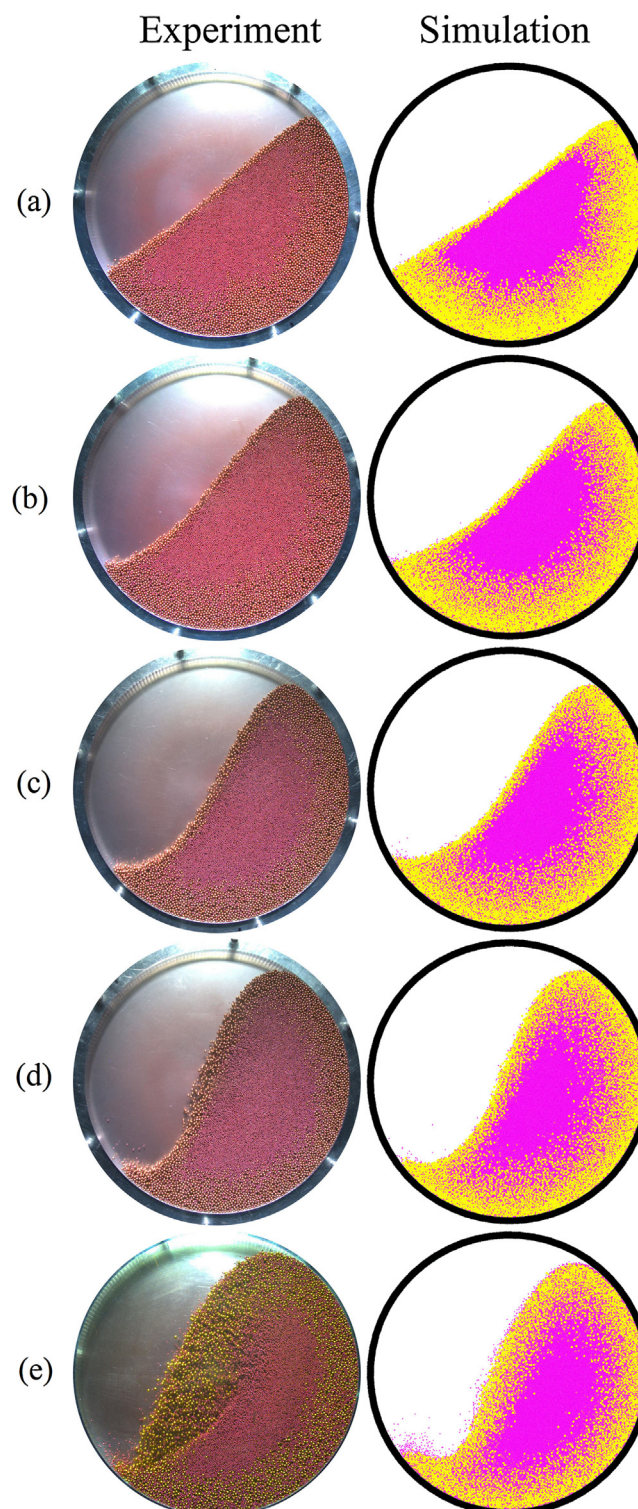


Fig. 6. Snapshots of the stable state in the rotating drum with volume ratio of 1 for different rotational speeds: (a) 4 rpm, (b) 8 rpm, (c) 16 rpm, (d) 32 rpm, and (e) 56 rpm.

ers a brighter area of approximately 4 pixels. The average gray value of the bright point is chosen based on a 150×150 -pixel subimage extracted from the original image; two sample subimages are shown in Figs. 2(a) and (b).

Step 5: Calculation—After thresholds were determined, the different-sized brighter areas were identified and located using one procedure of the designed code. The coordinates of the brightest pixel among the brighter areas were determined as the coordi-

nates of the corresponding large and small particles. The results of this identification are shown as a subimage in Fig. 2(c). The whole identification result for the particle field is given in Fig. 3.

We examined the accuracy of this image analysis method. Nineteen 150×150 -pixel subimage samples (from experiments) were selected randomly. These samples included particle systems of high concentration in a slow rotating drum and particle systems of relatively low concentration in a fast-rotating drum. The total number

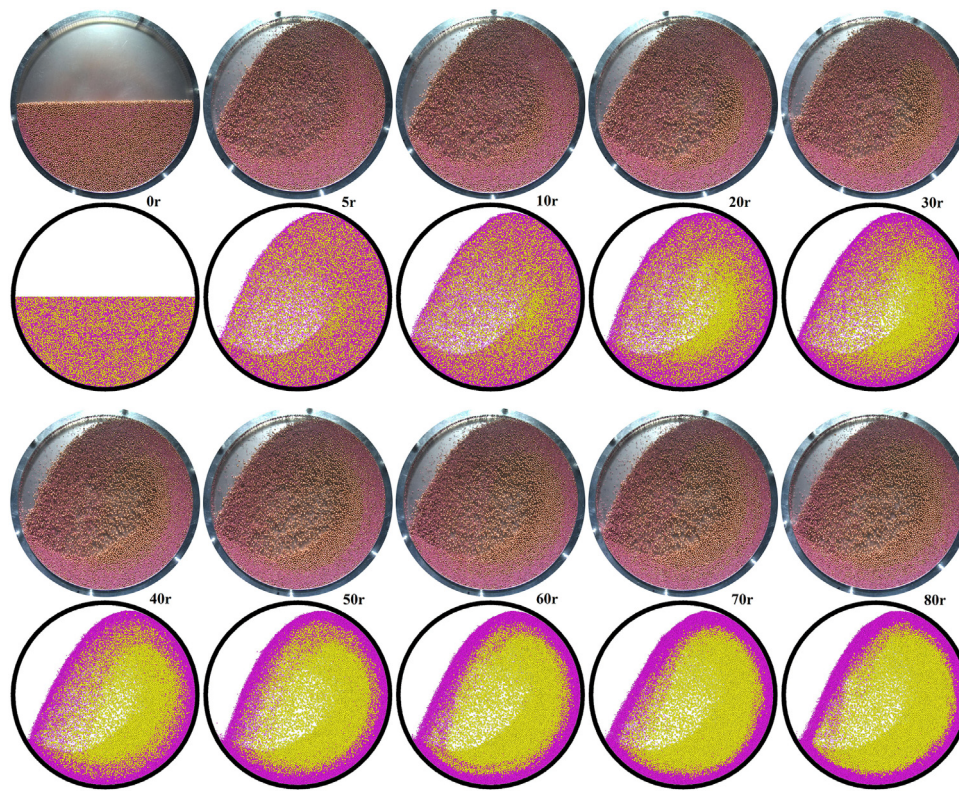


Fig. 7. Evolution process of reverse segregation from experiments and simulations.

of large particles and small particles in these samples were 1540 and 5234, respectively, and the identification results obtained using the above described image analysis method were 1547 and 5271, respectively. The recognition rates for the large and small particles were 99.55% and 99.29%. Moreover, the average error rate for the small particle concentration is 1.74%. Hence, from the definition of the Lacey mixing index (Lacey, 1954), the expected error was 0.87%. The errors of this image analysis method mainly come from non-uniform illumination. Recognizing bright points of different sizes as the major characteristic for identifying particles of different sizes ensures the technique is remarkably noise-tolerant and robust. In addition, this image analysis method can be applied to particle recognition and location over a wide range of particle concentrations.

Results and discussion

Evaluation of degree of segregation

To investigate segregation, several methods have been developed to evaluate the segregation or mixing state (Wen, Liu, Liu, & Shao, 2015). The Lacey mixing index, which is widely used in scientific research and industrial production, is employed in this study. To determine this index, the space occupied by particles needs to be divided in the simulations and the experiments. The grid partition and filling rate of the drum is presented in Fig. 4. Because the number of particles in each grid may differ significantly, a weighted Lacey mixing index was developed

$$M = \sqrt{\frac{1}{k} \sum_{i=1}^{N_t} k_i (a_i - \bar{a})}, \quad (8)$$

where N_t is the total sample size, a_i is the volume fraction of any of the two particle types, and \bar{a} is the over-all proportion of the

particle types. A normalization factor k is defined,

$$k = \sum_{i=1}^{N_t} k_i, \quad (9)$$

where k_i is the weight of the sample determined from

$$k_i = \frac{N_i}{N}, \quad (10)$$

where N_i is the number of equivalent particles in the sample, and N is the sum of the number of equivalent particles in all samples. The so-called equivalent particles are based on small particles; the equivalent number ratio of one large particle to one small particle is the cube of the diameter ratio. For example, if the diameter of the large particle is twice that of the small particle, one big particle is equivalent to eight small particles.

Validation

To validate the DEM, experiments of different-sized particles in the drum at different rotational speeds were performed. From the definition of Froude number F_r ($F_r = r\omega^2/g$) and the range of the slumping regime, petals (forming the sun pattern) occur at the rotational speed of 2 rpm. In the experiment, most of the small particles segregate and move into the inner core after one revolution, consistent with the reports in other papers (Jain, Ottino, & Lueptow, 2005; Nityanand et al., 1986). A predictable sun pattern (Fig. 5(a)) is formed ten revolutions later. The average dynamic repose angle is 34.5° ; in the experiment, seven petals formed. In simulations, small particles also segregate and gather in the inner core after one revolution, the average dynamic repose angle being about 33.5° . When ten revolutions were completed, seven petals were also observed (Fig. 5(b)).

With rotational speeds ranging from 4 to 56 rpm, stable-state macroscopic comparisons between simulations and experiments

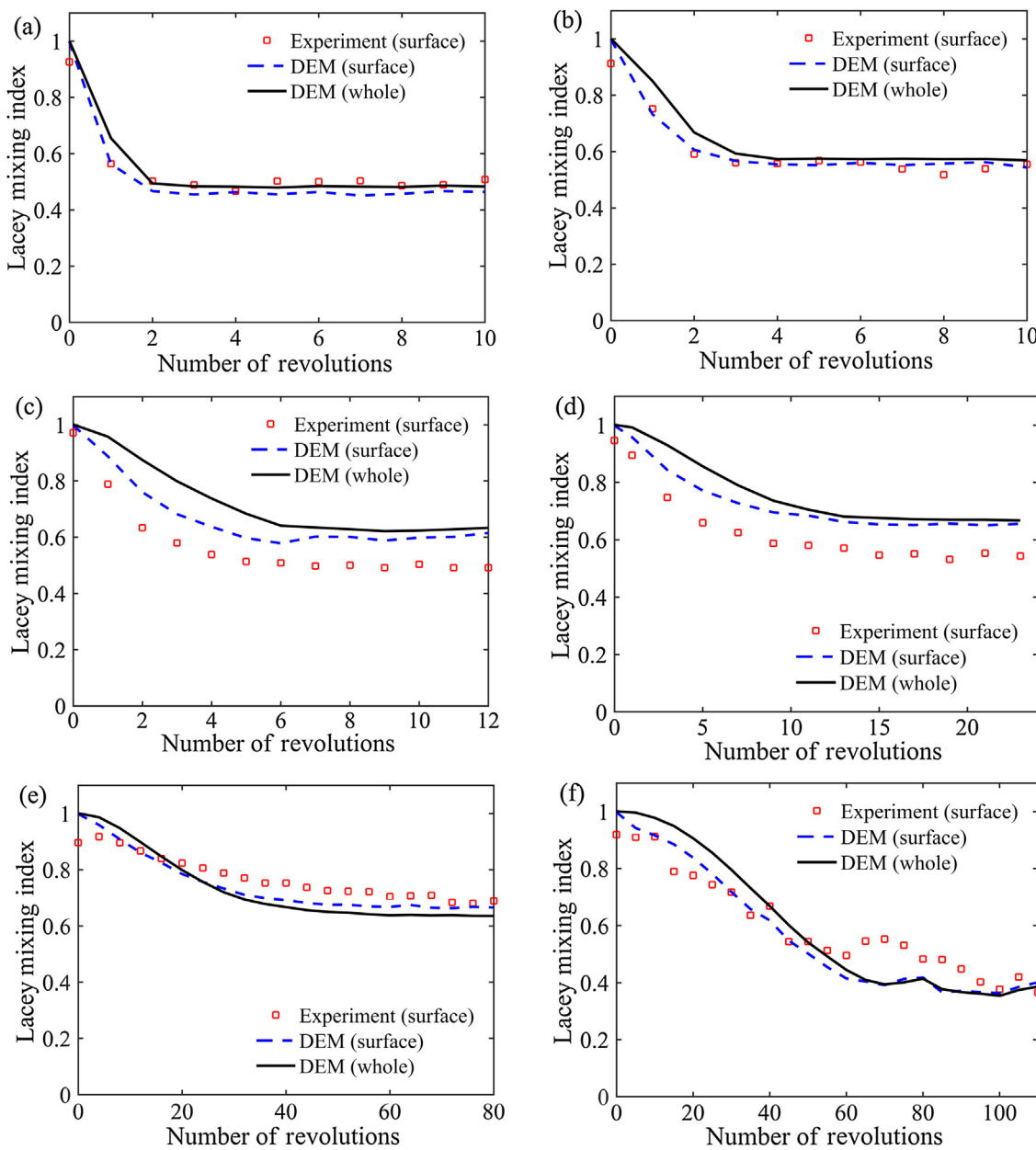


Fig. 8. Dependence of the Lacey mixing index with the number of revolutions at different rotational speeds: (a) 4 rpm, (b) 8 rpm, (c) 16 rpm, (d) 32 rpm, (e) 56 rpm, and (f) 80 rpm with volume ratio of 1.

were also made (Fig. 6). We found that the dynamic repose angle or the profile of the free particle surface and the distributions of large and small particles obtained from experiments matched well with those in simulations.

For a fixed rotational speed of 80 rpm, dynamic state comparisons between simulations and experiments were made (Fig. 7). In this instance, reverse segregation appears in both experiments and simulations. Moreover, the profile of the free particle surface and the distribution of large particles in each experiment were consistent with those in the corresponding simulation.

Aside from these qualitative and visualized comparisons, contrasts in the Lacey mixing index between simulations and experiments were also conducted to validate the DEM model. The Lacey mixing index calculated from particles at the surface of the drum in the experiments (dispersed symbols) is based on the image analysis technique. In simulations, the Lacey mixing index calculated from particles at the surface (dash line) of the drum and from all the particles (solid line) in the drum was obtained based on infor-

mation (size and position of each particle) outputted from the DEM simulation (Fig. 8). In general, the discrete points align on the dash line; that is, the degree of mixing from each simulation basically matches that of the experiment, which means the adopted DEM model is reliable.

Differences in the degree of mixing between surface and the bulk

To find out more, the differences in the degree of mixing between surface and the bulk were noted. In the rolling and cascading regimes, the degree of mixing presented at the surface seems to underestimate the degree of mixing in the bulk (Fig. 8(a)-(d)), and the difference tends to grow slowly as segregation evolves until the degree of mixing reaches equilibrium. The differences are in agreement with the relative errors between surface mixing and bulk mixing of the short drum reported in Liu et al. (2017). In the cataracting regime, the trend remains the same before the critical point, where the lines meet, is reached. Beyond this point, the

degree of mixing of the surface seems to be overestimated (Fig. 8(e)) or almost equal to the degree of mixing in the bulk (Fig. 8(f)).

Effect of rotational speed and volume ratio on segregation

With increasing rotational speed, there exist different transverse flow regimes (sliding, surging, slumping, rolling, cascading, cataracting, centrifuging) of the particles in a rotating drum (Mellmann, 2001). Particle flow is one common way to give rise to segregation. Results from simulation and experiment for various particle flow regimes were used to investigate radial segregation in a thin drum.

To better present the effect of rotational speed on the final mixing state, its evolution for different rotational speeds is integrated in one figure (Fig. 9). In the rolling regime (4 rpm) and cascading regime (8, 16, and 32 rpm), the degree of segregation decreases with increasing rotational speed, as evident from snapshots given in Fig. 6(a)–(d). Moreover, this trend is not valid in the cataracting regime (56 and 80 rpm); that is, the degree of segregation does not decrease with increasing rotational speed. Once the rotational speed reaches a critical value, reverse segregation occurs and the degree of segregation becomes rather high. Furthermore, the trend for the variation in the stable degree of mixing with rotational speed agrees with Fig. 7 of Arntz et al. (2008).

Why does the degree of final segregation decrease with increasing rotational speed in both the rolling and cascading regimes? The stable segregation state in the rotating drum is obtained from the interaction of segregation and diffusion. The percolation of small particles is the cause of segregation. The associated percolation theory (Bridgwater, Foo, & Stephens, 1985; Cooke & Bridgwater, 1979; Fan et al., 2014) was studied by some researchers and the percolation is proportional to the shear rate of the flow layer. The velocity fields of the particles in the drum (Fig. 10) show that in the rolling regime, there is a lens-like flowing layer on a static granular bed, which was also reported in Herz et al. (2009). With increasing

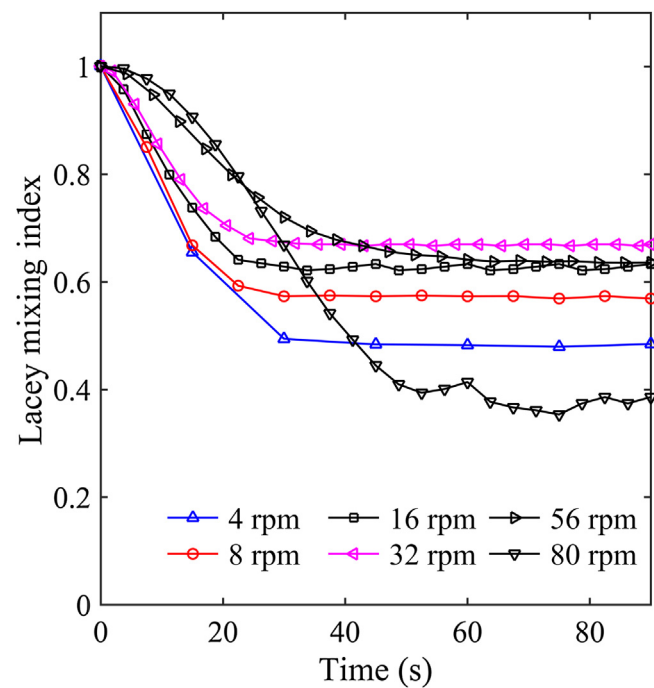


Fig. 9. Time evolution of the mixing index at different rotational speeds with volume ratio of 1.

ing rotational speed, the shape of free surface changes from flat to curved, and the thickness of the active layer experiences a change from thin to thick, as observed in the previous experiments (Nafsun et al., 2017). After obtaining the velocity fields, velocity profiles that reflect the shear rate were extracted from representative fields one centimeter wide rectangular areas containing the drum's center (see Fig. 10(d)). Fig. 11 gives a plot of the velocity profile showing

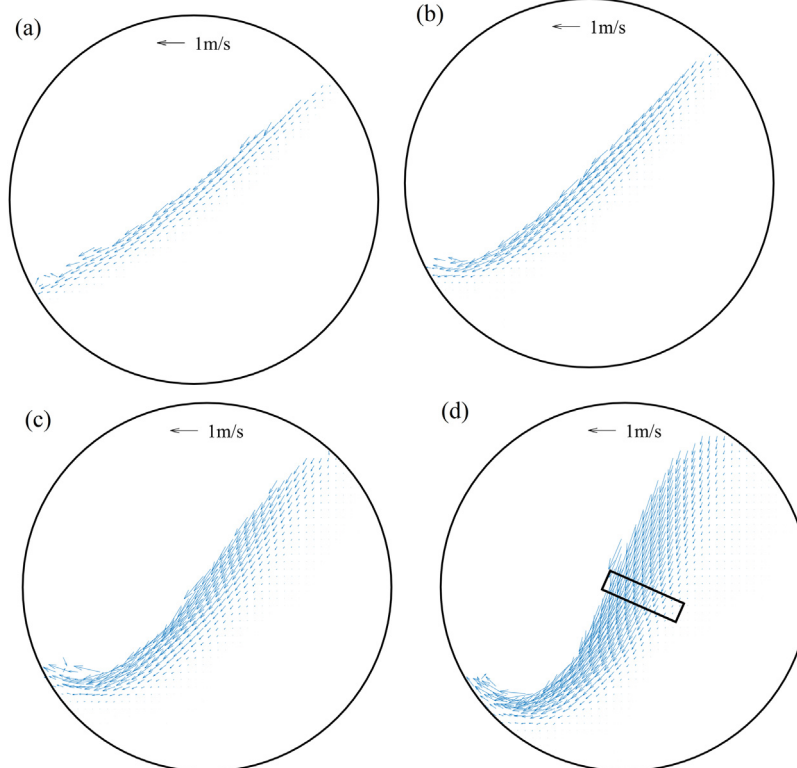


Fig. 10. Velocity fields with volume ratio of 1 at different rotational speeds: (a) 4 rpm, (b) 8 rpm, (c) 16 rpm, and (d) 32 rpm.

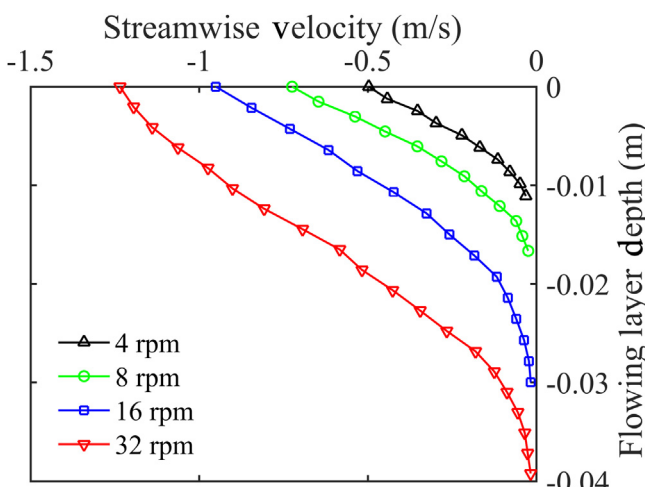


Fig. 11. Velocity profile in the central part of the active layer.

that shear rates do not vary much, which means percolation is not enhanced with increasing rotational speed and the other factors such as diffusion needs to be examined. The granular temperature (Chou & Hsiao, 2011) is defined as the specific fluctuations in kinetic energy of the granular flow, which means the bigger the granular temperature, the greater the diffusion of particles in the flowing layer. Granular temperatures were also extracted from the area where the velocity profiles were obtained (Fig. 12). It can be seen that the granular temperature increases with increasing rotational speed. That is, diffusion becomes more intense when the rotational speed is faster. Thus, the reason why the degree of final segregation decreases with increasing rotational speed for both rolling and cascading regimes is that percolation remains the same, but diffusion becomes stronger.

Fig. 13 shows the time evolution of the degree of mixing at different rotational speeds with volume ratios of 1/2 and 1/3. Combined with Fig. 9, the volume ratio shows different effects on the degree of segregation in different flow regimes. In the rolling and cascading regimes, the volume ratio has little influence on the degree of segregation, whereas in the cataracting regime, the volume ratio has a significant impact on the degree of segregation (Figs. 9 and 13, solid lines with right-pointing and inverted triangles). The degree of final segregation at 56 rpm is not necessarily lower than that at 32 rpm. Moreover, in the cataracting regime the degree of segregation decreases with decreasing volume ratio—the lower the volume ratio, the more small particles diffuse among the large particles (see Fig. 14).

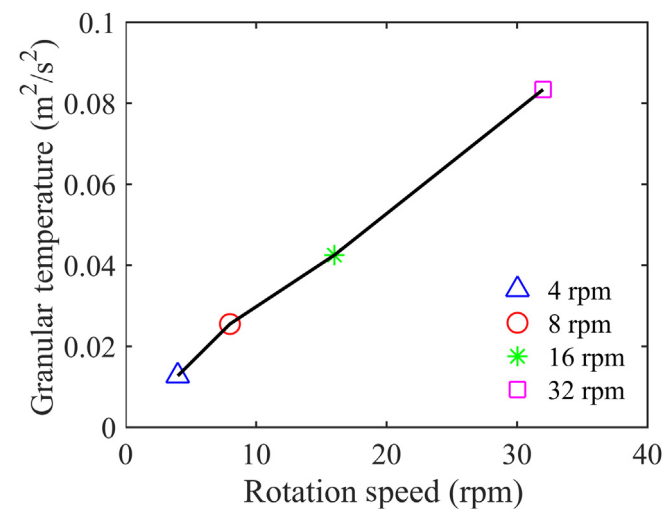


Fig. 12. Granular temperature in the central part of the active layer.

In the rolling and cascading regimes (Figs. 9 and 13), the time required to achieve a final segregation state is not significantly related to the rotational speed. Compared with the rolling and cascading regimes, the time to reach the steady segregation state in the cataracting regime is longer.

Mechanism of reverse segregation

In Nityanand et al. (1986) and Turner and Nakagawa (2000), reverse segregation of small particles was found to be easily centrifuged towards the wall of the cylinder. Arntz et al. (2008) attributed this behavior to the low particle concentration in the impinging area and refuted the improper interpretation of reverse segregation given by Nityanand et al. Whereas the demonstration of Arntz and his collaborators is reasonable, it is not complete because their simulation had an insufficient number of particles. Here, we present our explanation for the mechanism of reverse segregation.

From the velocity fields (Figs. 15(a) and (b)), there exists even in the cataracting regime an active layer on the passive particle bed. The difference from the rolling and cascading regimes is that its location and area has changed. Large particles still segregate out in the top active layer. Nevertheless, why does not reverse segregation occur at 56 rpm? The reason is that at 56 rpm, an impinging area where intense collisions occur does not emerge, whereas at 80 rpm large particles segregating to the top active layer are obstructed by an impinging area. That is, they cannot pass through the impinging

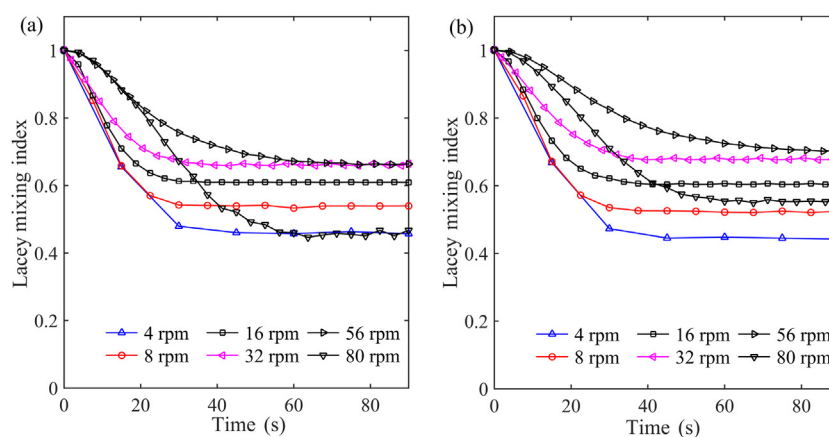


Fig. 13. Time evolution of the mixing index at different rotational speeds with volume ratios of (a) 1/2 and (b) 1/3.

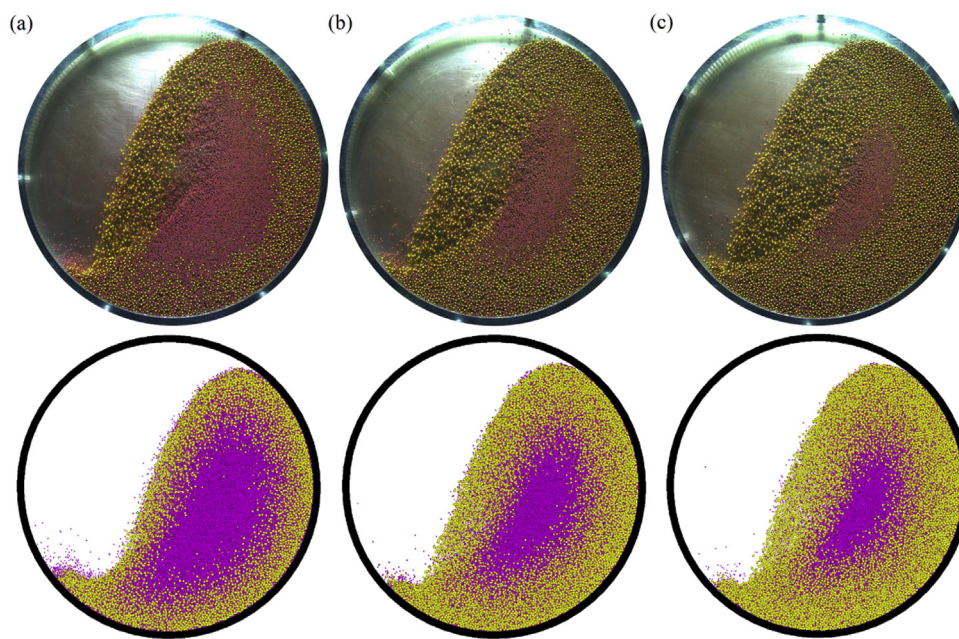


Fig. 14. Snapshots of the steady state obtained from experiments and simulations at 56 rpm with different volume ratios: (a) 1, (b) 1/2, and (c) 1/3.

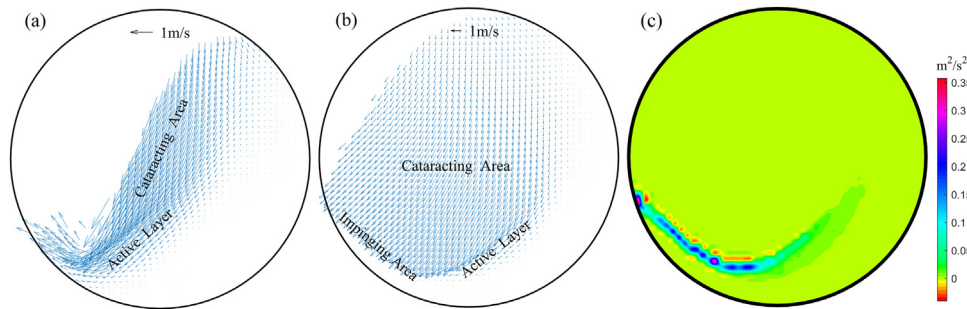


Fig. 15. Reverse segregation: (a) and (b) velocity field distributions at 56 and 80 rpm with volume ratio of 1, (c) granular temperature field corresponding to (b).

area to the periphery of the drum. The necessary condition for no reverse segregation is that the large particles can reach the periphery of the drum. In addition, the presence of this impinging area leads to a particle concentration that is relatively low in this region, enabling small particles to percolate. As granular temperature is defined as a specific fluctuation in kinetic energy of the granular flow, it is also understood that the higher the granular temperature, the greater the fluctuation in particle movement and the smaller is the particle concentration. Therefore, the concentration of the particles is dependent on the granular temperature (see Fig. 15(c) for 80 rpm). Note also that the granular temperature in the impinging area is significantly higher than other areas, and thus it can be inferred that the particle concentration in this region is relatively small. Therefore, the flowing layer, the impinging area, and the low particle concentration together contribute to reverse segregation in the cataracting regime.

Conclusions

A linear elastic damping DEM model was adopted and an image analysis performed to investigate segregation of particles in a rotating drum was applied. Simulations and experiments with a full range of drum speeds and different volume ratios were conducted as well.

The applied image analysis method, which recognizes and locates particles of different sizes directly, is robust and accurate.

It has proved to be a powerful tool when investigating the segregation of different-sized particles in the rotating drum. With this imaging technique, the DEM model and code were validated. The flow behaviors and segregation of bi-disperse particle systems were effectively and accurately simulated using the code.

The simulation and experiment results show that in the rolling and cascading regimes, the degree of segregation decreases with increasing rotational speed, whereas the volume ratio shows little influence on segregation. In the cataracting regime, the degree of segregation decreases with decreasing volume ratio, and when rotational speed exceeds a critical value reverse segregation will occur. By analyzing the velocity and granular temperature fields, the mechanism of reverse segregation was clarified.

The simulation method compensates for the disadvantage of the experiment method—namely, the difficulty to obtain overall information of particles in the apparatus. The experimental method helped to verify the reliability of the simulation results. Moreover, combining these two approaches proved helpful in investigating these particle systems.

Conflict of interest

The authors declare that they have no conflicts of interest.

Acknowledgements

We acknowledge the support of the National Natural Science Foundation of China (NSFC, Grant Nos. 21476193, 51741608).

References

- Alchikh-Sulaiman, B., Alian, M., Ein-Mozaffari, F., Lohi, A., & Upreti, S. R. (2016). Using the discrete element method to assess the mixing of polydisperse solid particles in a rotary drum. *Particuology*, 25, 133–142.
- Arntz, M., M. H. D., Beeltink, H. H., den Otter, W. K., Briels, W. J., & Boom, R. M. (2014). Segregation of granular particles by mass, radius, and density in a horizontal rotating drum. *AIChE Journal*, 60(1), 50–59.
- Arntz, M. M. H. D., den Otter, W. K., Briels, W. J., Bussmann, P. J. T., Beeltink, H. H., & Boom, R. M. (2008). Granular mixing and segregation in a horizontal rotating drum: A simulation study on the impact of rotational speed and fill level. *AIChE Journal*, 54(12), 3133–3145.
- Bridgwater, J. (2012). Mixing of powders and granular materials by mechanical means—A perspective. *Particuology*, 10(4), 397–427.
- Bridgwater, J., Foo, W. S., & Stephens, D. J. (1985). Particle mixing and segregation in failure zones—theory and experiment. *Powder Technology*, 41(2), 147–158.
- Chou, S. H., & Hsiao, S. S. (2011). Experimental analysis of the dynamic properties of wet granular matter in a rotating drum. *Powder Technology*, 214, 491–499.
- Cooke, M. H., & Bridgwater, J. (1979). Intercrystallite percolation: A statistical mechanical interpretation. *Industrial and Engineering Chemistry Fundamentals*, 18(1), 25–27.
- Cundall, P. A., & Strack, O. D. L. (1979). A discrete numerical model for granular assemblies. *Géotechnique*, 29(1), 47–65.
- Dury, C. M., & Ristow, G. H. (1997). Radial segregation in a two-dimensional rotating drum. *Journal de Physique I*, 7, 737–745.
- Fan, Y., Schlick, C. P., Umbaranwar, P. B., Ottino, J. M., & Lueptow, R. M. (2014). Modelling size segregation of granular materials: The roles of segregation, advection and diffusion. *Journal of Fluid Mechanics*, 741, 252–279.
- Fedor, S. J., & Ottino, J. M. (2005). Mixing and segregation of granular matter: Multi-lobe formation in time-periodic flows. *Journal of Fluid Mechanics*, 533, 223–236.
- Gray, J. M. N. T. (2010). Particle size segregation in granular avalanches: A brief review of recent progress. *AIP Conference Proceedings*, 1227(May (1)), 343–362. AIP.
- Gray, J. M. N. T., & Hutter, K. (1997). Pattern formation in granular avalanches. *Continuum Mechanics and Thermodynamics*, 9, 341–345.
- Hertz, H. (1896). *Miscellaneous papers*. London: Macmillan.
- Herz, F., Sonavane, Y., Specht, E., Bensmann, S., & Walzel, P. (2009). Mixing behaviour for the mass and heat of granular material in the agitated bed of rotating drums. *International Conference on Measurement and Control of Granular Materials*.
- Hill, K. M., Gioia, G., & Amaravadi, D. (2004). Radial segregation patterns in rotating granular mixtures: Waviness selection. *Physical Review Letters*, 93(22), 224301.
- Hill, K. M., Gioia, G., Amaravadi, D., & Winter, C. (2005). Moon patterns, sun patterns, and wave breaking in rotating granular mixtures. *Complexity*, 10(4), 79–86.
- Jain, N., Ottino, J. M., & Lueptow, R. M. (2002). An experimental study of the flowing granular layer in a rotating tumbler. *Physics of Fluids*, 14(2), 572–582.
- Jain, N., Ottino, J. M., & Lueptow, R. M. (2005a). Combined size and density segregation and mixing in noncircular tumblers. *Physical Review E*, 71(5), 051301.
- Jain, N., Ottino, J. M., & Lueptow, R. M. (2005b). Regimes of segregation and mixing in combined size and density granular systems: An experimental study. *Granular Matter*, 7, 69–81.
- Khakhar, D. V., McCarthy, J. J., Shinbrot, T., & Ottino, J. M. (1997). Transverse flow and mixing of granular materials in a rotating cylinder. *Physics of Fluids*, 9, 31–43.
- Komossa, H., Wirtz, S., Scherer, V., Herz, F., & Specht, E. (2014). Transversal bed motion in rotating drums using spherical particles: Comparison of experiments with DEM simulations. *Powder Technology*, 264, 96–104.
- Lacey, P. M. C. (1954). Developments in the theory of particle mixing. *Journal of Applied Chemistry*, 4(5), 257–268.
- Liu, X., Hu, Z., Wu, W., Zhan, J., Herz, F., & Specht, E. (2017). DEM study on the surface mixing and whole mixing of granular materials in rotary drums. *Powder Technology*, 315, 438–444.
- McCarthy, J. J., Shinbrot, T., Metcalfe, G., Wolf, J. E., & Ottino, J. M. (1996). Mixing of granular materials in slowly rotated containers. *AIChE Journal*, 42(12), 3351–3363.
- Mellmann, J. (2001). The transverse motion of solids in rotating cylinders—Forms of motion and transition behavior. *Powder Technology*, 118, 251–270.
- Metcalfe, G., Shinbrot, T., McCarthy, J. J., & Ottino, J. M. (1995). Avalanche mixing of granular solids. *Nature*, 374, 39–41.
- Mindlin, R. D. (1949). Compliance of elastic bodies in contact. *Journal of Applied Mechanics*, 16, 259–268.
- Mindlin, R. D., & Deresiewicz, H. (1953). Elastic spheres in contact under varying oblique forces. *Journal of Applied Mechanics—Transactions of the ASME*, 20(3), 327–344.
- Nafsun, A. I., Herz, F., Specht, E., Komossa, H., Wirtz, S., Scherer, V., et al. (2017). Thermal bed mixing in rotary drums for different operational parameters. *Chemical Engineering Science*, 160, 346–353.
- Nityanand, N., Manley, B., & Henein, H. (1986). An analysis of radial segregation for different sized spherical solids in rotary cylinders. *Metallurgical Transactions B*, 17B, 247–257.
- Ottino, J. M., & Lueptow, R. M. (2008). On mixing and demixing. *Science*, 319(5865), 912–913.
- Pereira, G. G., Pucilowski, S., Liffman, K., & Cleary, P. W. (2011). Streak patterns in binary granular media in a rotating drum. *Applied Mathematical Modelling*, 35, 1638–1646.
- Prigozhin, L., & Kalman, H. (1998). Radial mixing and segregation of a binary mixture in a rotating drum: Model and experiment. *Physical Review E*, 57(2), 2073–2080.
- Santomaso, A., Olivi, M., & Canu, P. (2005). Mixing kinetics of granular materials in drums operated in rolling and cataracting regime. *Powder Technology*, 152, 41–51.
- Thomas, N. (2000). Reverse and intermediate segregation of large beads in dry granular media. *Physical Review E*, 62(1), 961–974.
- Thornton, C., Cummins, S. J., & Cleary, P. W. (2013). An investigation of the comparative behaviour of alternative contact force models during inelastic collisions. *Powder Technology*, 233, 30–46.
- Ting, J. M., & Corkum, B. T. (1992). Computational laboratory for discrete element geomechanics. *Journal of Computing in Civil Engineering*, 6, 129–146.
- Turner, J. L., & Nakagawa, M. (2000). Particle mixing in a nearly filled horizontal cylinder through phase inversion. *Powder Technology*, 113, 119–123.
- Walton, O. R. (1993). Numerical simulation of inclined chute flows of monodisperse, inelastic, frictional spheres. *Mechanics of Materials*, 16, 239–247.
- Walton, O. R., & Braun, R. L. (1986). Viscosity, granular-temperature, and stress calculations for shearing assemblies of inelastic, frictional disks. *Journal of Rheology*, 30, 949–980.
- Wen, Y., Liu, M., Liu, B., & Shao, Y. (2015). Comparative study on the characterization method of particle mixing index using DEM method. *Procedia Engineering*, 102, 1630–1642.
- Zuriguel, I., Gray, J. M. N. T., Peixinho, J., & Mullin, T. (2006). Pattern selection by a granular wave in a rotating drum. *Physical Review E*, 73(6), 061302.
- Zuriguel, I., Peixinho, J., & Mullin, T. (2009). Segregation pattern competition in a thin rotating drum. *Physical Review E*, 79(5), 051303.